# Streaked speckle in $Cu_3Au$ coherent x-ray diffraction

J. A. Pitney,[1] I. K. Robinson,[1] I. A. Vartaniants,[1,2] R. Appleton,[1] and C. P. Flynn[1]
[1]*Department of Physics, University of Illinois, Urbana, Illinois 61801*
[2]*Institute of Crystallography RAS, Leninsky Prospekt 59, 117333 Moscow, Russia*
(Received 2 June 2000)

Coherent x-ray diffraction from the binary alloy $Cu_3Au$ has speckled superstructure Bragg reflections due to its antiphase domain structure. For nonspecular superstructure reflections, it is possible to vary the diffraction geometry through a range of incidence and exit angles. Under grazing-exit conditions on a prepared $Cu_3Au(111)$ thin-film sample, the superstructure speckles are found to become highly elongated and rotated on the detector. A detailed geometrical explanation of this behavior is developed to explain the effect.

Coherent x-ray diffraction (CXD) has the marvelous virtue that the diffraction pattern is the exact Fourier transform of the object under investigation without the ensemble averaging associated with conventional x-ray scattering. The connection with microstructure was originally discovered in $Cu_3Au$ by Sutton *et al.*[1] and further explored in polymer films coated with gold,[2] in semiconductor multilayers,[3] and for probing the morphology of silicon wafers[4] and the porous structure of aerogel.[5] The sensitivity to local structure has also been utilized in several recent intensity fluctuation experiments: critical fluctuations of the binary alloy $Fe_3Al$;[6] diffusion of colloidal particles of gold,[7] palladium,[8] and antimony oxide;[9] equilibrium dynamics of block-copolymer micelles;[10] and nonequilibrium dynamics of phase separation in a sodium borosilicate glass.[11] Here we are interested in the original application of CXD, which utilizes its inherent sensitivity to the structure and morphology of complex heterogeneous materials to preserve information about localized structures. It has been suggested by Sayre[12] that the continuous property of this diffraction, coupled with iterative image reconstruction techniques, may be used as a form of x-ray microscopy. This has been recently demonstrated for soft x rays in a model system by Miao *et al.*[13]

The complete diffraction pattern of a small crystalline object, as can be measured by the CXD experiment, is the combination of multiple factors, only one of which is the structure factor of the arrangement of the atoms within its unit cell. The distribution of the diffraction pattern in reciprocal space is necessarily related to the shape of the object in real space, through Fourier transformation. Complex materials can be considered to be a coherent superposition of simpler objects, whose structures can be broken down hierarchically. The diffraction pattern contains the information about each distinct object as well as the interference between them. Today's third-generation high-brightness synchrotron x-ray sources are sufficiently coherent to investigate microstructure in this way. Here we explore the detailed nature of the diffraction pattern of a simple, yet nontrivial, material that is a thin film of disordered binary metallic alloy. To enrich the available information, we investigate for the possibility of varying the x-ray geometrical degrees of freedom to obtain different cross-sectional views of the immediate vicinity of a single point of reciprocal space. As we will show, this information can be used to extract three-dimensional details about the shape of the diffraction and hence about the distribution of the scattering objects.

The sample we examined was a slab of $Cu_3Au$ crystal grown using the molecular beam epitaxy (MBE) method to produce a well-defined free surface, along its crystallographic (111) plane. Large antiphase domains are known to form in this material when it is suitably annealed. The antiphase domains correspond to the occupation by Au atoms of one of four simple-cubic (sc) sublattices of the face-centered cubic (fcc) underlying crystal lattice, while Cu atoms occupy the remaining three sublattices. This gives rise to superlattice reflections in the diffraction pattern. Abrupt domain boundaries occur between domains in which the Au switches from one sublattice to another; the phase of the structure factor of the superlattice (i.e., sc but not fcc) reciprocal-lattice points reverses upon crossing certain domain boundaries.[14] In conventional (incoherent) diffraction, these ''antiphase'' domains lead to broadening of these diffraction spots;[14] in CXD this leads to a ''speckled'' pattern.[1]

The arrangement of antiphase domain shapes and sizes in bulk $Cu_3Au$ is known from examination of thin sections using dark-field electron microscopy.[15] A quadrangular appearance is found because of the tendency of domain walls to adopt {100} orientations. It is believed that the same arrangement exists right up to the surface layer of a finite crystal, since the bulk and (lateral) surface correlation lengths show the same equilibrium scaling behavior with temperature in the vicinity of the disordering temperature.[16] This happens in spite of the strong tendency of Au to segregate to the (100) surface used in those studies and the fact that this favors two of the four possible sublattices there. At a (111) surface, where the segregation cannot bias the sublattice distribution, less is known about the distribution of antiphase domains; the surface-sensitive diffraction experiments resulted in a two-component line shape that was interpreted to be caused by heterophase fluctuations.[17] For the (111) case, the situation is more complicated because the preferred domain-wall orientation is no longer perpendicular to the surface.

The $Cu_3Au$ sample we studied had a $(11\bar{2}0)$-oriented sapphire substrate that was annealed at 1050 °C for 2 h, before depositing by MBE a 500–1000-Å-thick Nb buffer layer at 900 °C and 0.2 Å/s. The Nb had a (110) orientation. The

 

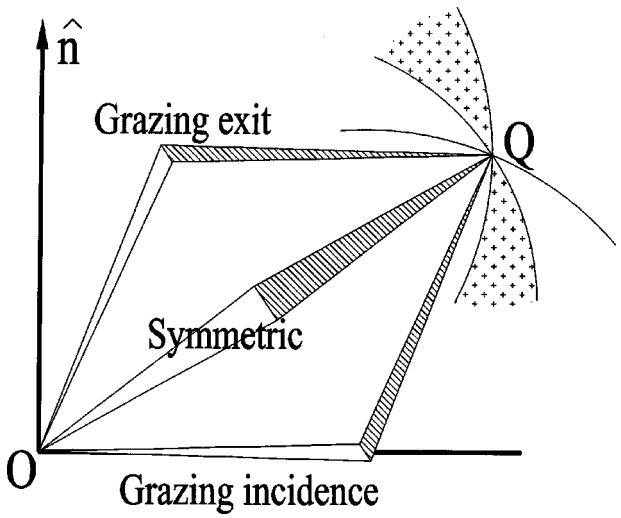


FIG. 1. Illustration of the diffraction geometry of the Ewald construction under grazing incidence, symmetric, and grazing exit geometries. *OQ* denotes the vector $\mathbf{q}=\mathbf{k}_f-\mathbf{k}_i$, which lies in the plane of the page, as does the surface-normal direction which is denoted $\hat{\mathbf{n}}$. The beams representing $\mathbf{k}_f$ and $\mathbf{k}_i$ are directed towards the page and are drawn as shaded and unshaded triangles to imply perspective. The images seen in the detector are the section of the Ewald sphere drawn as arcs passing through *Q*, one for each case.

temperature was reduced to 330 °C before Cu and Au were codeposited to form a 2000-Å-thick film of (111)-oriented $Cu_3Au$. To anneal out any composition gradients, the temperature was raised to 450 °C for 15 min; then, the sample was annealed at 360 °C for 12 h and at 300 °C for 48 h. This annealing schedule resulted in antiphase domains with a characteristic size of 400 Å, as determined by the width of the superstructure peaks in an incoherent diffraction measurement. Twin domains, usually associated with different fcc stacking sequences of the $Cu_3Au$ on the Nb(110) buffer layer,[19] were found to be in the 10–100-$\mu$m size range, so it was possible to perform the experiment within a single twin.

The measurements were performed at the Advanced Photon Source (APS) undulator beamline 33-ID. The beam was passed through a double-crystal Si(111) monochromator, which provided a bandwidth of $\Delta\lambda/\lambda\approx 2\times 10^{-4}$, giving a longitudinal (temporal) coherence length of $\xi_{\parallel}\approx 7300$ Å at the selected photon energy $E=8.5$ keV. The undulator beam has a source size of 350 $\mu$m (Gaussian $\sigma$ width) in the horizontal and 50 $\mu$m in the vertical directions,[20] so that, at the experiment, a distance $D=40$ m downstream, the spatial coherence lengths are $\xi_{\text{horiz}}\approx 5\ \mu$m and $\xi_{\text{vert}}\approx 33\ \mu$m. The beam was therefore passed through a 5 $\mu$m$\times$5 $\mu$m square aperture to select a suitably coherent beam. This aperture was formed by a crossed pair of slits with a rollerblade design, which allowed us to set the gap and the position of each slit with about 1-$\mu$m precision with good reproducability.[21] The slits were located 10 cm from the sample position. The sample and detector were oriented on a standard four-circle Huber diffractometer with a vertical scattering plane. We acquired diffraction patterns with a Princeton Instruments charge coupled device (CCD) detector with pixels measuring 22.5 $\mu$m square, located 2.8 m from the sample.

Coherent diffraction experiments were carried out in the extended-face reflection geometry,[14] and we took advantage of the CCD area detector to provide simultaneous detection of multiple points on the Ewald sphere. The resulting image on the detector is a spherical cut, intersecting the point of interest in reciprocal space illustrated in Fig. 1. For x rays of a given energy, the direction of this cut is determined by a single degree of freedom, which is the rotation of the sample about the fixed momentum transfer vector. For a large slab-shaped sample in reflection (''Bragg'' geometry), such as ours, that range of rotation is limited by the geometrical constraint that neither the incident nor exit beam may be occluded by the surface. The choice of diffraction geometry is described in Fig. 1, which shows three cases, the symmetric, grazing-incidence and grazing-exit extremes. Within the allowed range, the geometry variation can be used for three-dimensional mapping of the coherent diffraction pattern, suggested by the shading in Fig. 1. This mapping is exploited fully in the work reported here. We investigated the (100) reflection of a (111) sample at 8.5 keV, for which the angle of incidence onto the sample surface, $\alpha_i$, can be varied from 0° to 13.1°. This causes the exit angle $\alpha_f$, to range from 13.1° down to 0°. We also measured the (101) reflection, for which the range in angles is from 0° to 26.1°. The absorption length of 8.5-keV x rays in $Cu_3Au$ is 7.5 $\mu$m, so the illuminated thickness of the sample only starts to become limited by penetration when $\alpha_i$ or $\alpha_f$ reaches 1°.

Figure 2 shows examples of the CCD diffraction patterns, in which a dramatic change can be seen as the diffraction geometry is systematically varied. The pronounced streaking in the top panel, measured under grazing-exit angle conditions, is noteworthy. The slight shift and splitting of the intensity distribution in that pattern can be understood to be due to critical-angle effects,[22] but are not important here. There are several characteristic lengths visible in the data of Fig. 2. The envelope of the entire diffraction pattern has a size that is the reciprocal of the antiphase domain size; this was verified by opening the entrance slits to measure the conventional (incoherent) diffraction pattern from our sample and provided the characteristic size of 400 Å mentioned above.[18] The *width* of the speckles appears to be constant and is given by the reciprocal of the beam dimension, while the *length* of the speckles varies with incidence angle and seems to diverge in the grazing-exit situation: as grazing exit conditions are approached, this leads to a pronounced elongation of the speckle features. The *direction* of streaking on the detector also rotates with incidence angle, as seen. The data are for the (100) reflection, while analogous behavior was seen for the (101) reflection.

To understand this complicated behavior it is necessary to consider the mapping from the three-dimensional (3D) reciprocal-space region surrounding the Bragg point at which the diffraction pattern is formed onto the 2D section seen by the detector. This is accomplished by the Ewald sphere construction, illustrated in Fig. 1, in which the $\mathbf{k}_i$ (incident) and $\mathbf{k}_f$ (exit) wave vectors form two radii that define the Ewald sphere. The detector measures the small range of exit wave vectors that lie within a small patch on the sphere around $\mathbf{k}_f$. This patch is well-approximated by a tangent plane with its normal pointing along $\mathbf{k}_f$. As illustrated, the variation of $\alpha_i$ and $\alpha_f$ corresponds to a rotation about the fixed momentum-transfer vector, $\mathbf{q}=\mathbf{k}_f-\mathbf{k}_i$, denoted *OQ* in Fig. 1, between the grazing-incidence and grazing-exit limits shown. The

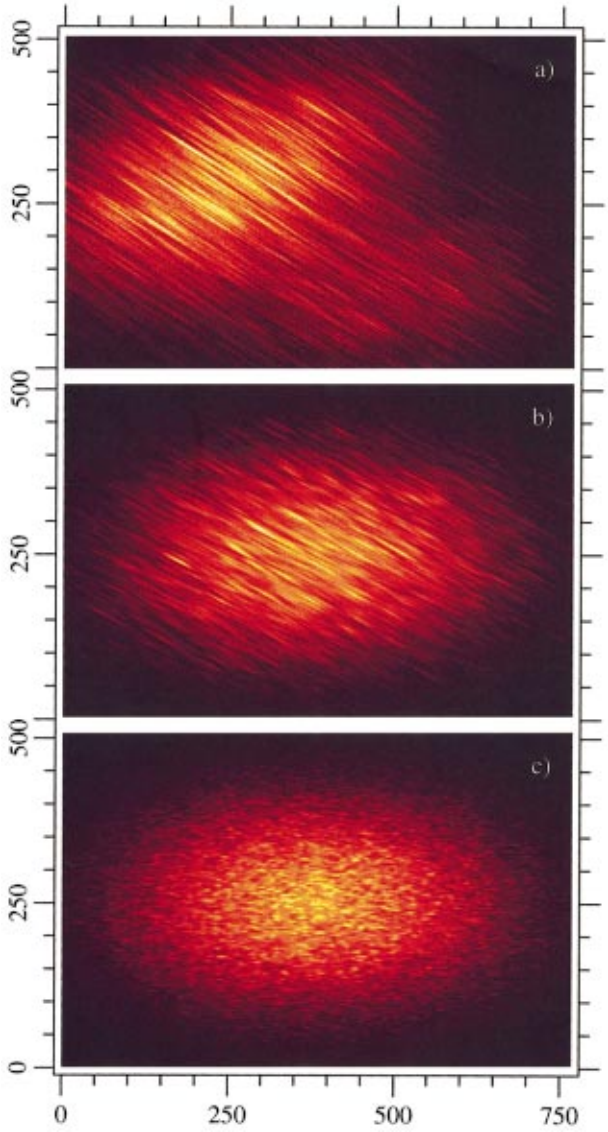


FIG. 2. (Color) CCD images of three CXD patterns, each measured at the (100) $Cu_3Au$ superstructure reflection. The axes are labeled in units of pixels, which are 22.5 $\mu$m wide, located 2.8 m from the sample. A 768×512 pixel region, covering 6.17 mrad×4.11 mrad, is shown for (a) $\alpha_i=12°$ or $\alpha_f=1°$, (b) $\alpha_i=10°$, $\alpha_f=3°$, and (c) $\alpha_i=7°$, $\alpha_f=6°$.

tangent plane thus slices through the 3D diffraction pattern at different angles. The grazing exit condition $\alpha_f \simeq 0$ is significant because it is the condition under which the tangent (detector) plane lies nearly parallel to the surface normal direction. Our observation of elongated speckles under just this situation suggests that the elongation direction is just the direction of the surface normal, as will be confirmed by our calculation below.

For a quantitative evaluation of the size and orientation of the speckles in each CCD image, we calculated the spatial autocorrelation function, $A(x',y')$, of the intensity $I(x,y)$ measured at the (discrete) pixel location $(x,y)$,

$$A(x',y')=\sum_{x,y=0}^{N} I(x,y)I(x+x',y+y'), \qquad (1)$$

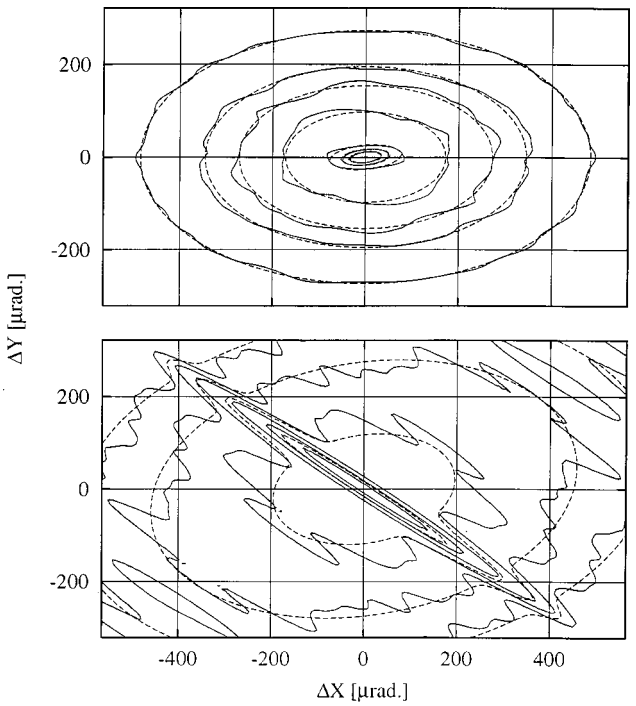


FIG. 3. Two examples of intensity autocorrelation functions for measured CXD patterns are shown as solid contour lines. The upper panel has $\alpha_i=2°$ and the lower one $\alpha_i=12°$, both for the (100) reflection. The plot shows the clear contributions of the broad background peak and the sharp peak near the origin, which is taken to be representative of the speckle characteristics of this image. Fits to the sum of two elliptical Gaussian functions are shown with dashed contours lines.

where $N$ is the size of the CCD array. The result was a sharp peak on top of a broad one, centered at the origin. The broad peak had the size and shape of the overall envelope of the speckle pattern, believed to be due to the contributions of the incoherent background and the speckle-to-speckle correlations. The single sharp peak, centered at the origin, had the size and shape of a ''typical'' speckle, because it mainly results from the internal correlations within each speckle. Figure 3 shows contours of two examples of autocorrelation functions, computed from an image of the (100) peak at $\alpha_i=2°(\alpha_f=11°)$ and $\alpha_i=12°(\alpha_f=1°)$. The autocorrelations were fit to a sum of two elliptical Gaussian functions, each one free to rotate about the origin, as shown in Fig. 3. From the fits to elliptical Gaussians, we obtained the characteristic orientation with respect to the horizontal as well as the major- and minor-axis $\sigma$ widths for each CXD pattern. The results are shown in Fig. 4 with open symbols for the (100) reflection and with filled symbols for the (101) reflection.

In order to model what is seen in the experiment, we first consider the intensity autocorrelation function to be an infinite cylindrical rod, of Gaussian cross section, centered at the origin with its axis oriented along the surface normal $\hat{\mathbf{n}}$ in reciprocal space. This represents the instrument response alone to an ideal two-dimensional object with finite illumination in real space, without any details of the sample. We use the Ewald construction to model its detection by the CCD, since this will be the same for both the intensity and its autocorrelation function. We will take $\hat{\mathbf{y}}$ to be in the direction perpendicular to $\mathbf{k}_f$ within the scattering plane (containing $\mathbf{k}_i$

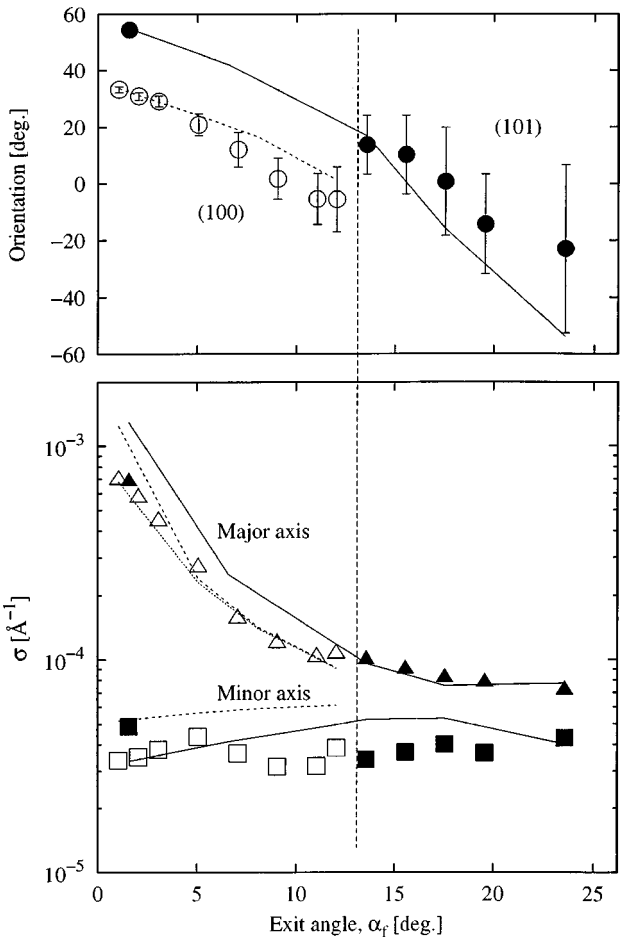


FIG. 4. Parameters describing the fits to the autocorrelation functions in Fig. 3, plotted as a function of the diffraction geometry. The orientation with respect to the horizontal $\hat{\mathbf{x}}$ axis as well as the major- and minor-axis $\sigma$ widths of the (100) reflection are shown as open symbols. Those of the (101) reflection are shown as filled symbols. The results of the model calculations are shown with dashed lines for the (100) reflection and with solid lines for the (101) case. For the major axis, two dashed curves are shown: the lower one (shorter dashes) is derived from the upper one by the correction for the thickness of the film.

and $\mathbf{k}_f$); this direction maps upward (positive $2\theta$) on the detector and in Fig. 2. We will take $\hat{\mathbf{x}}$ such that $\hat{\mathbf{y}}\times\hat{\mathbf{x}}$ points along $\mathbf{k}_f$. With this definition, the direction $\hat{\mathbf{x}}$ maps to the right on the detector and Fig. 2. Note that varying $\alpha_i$ also varies the orientation of $\mathbf{k}_f$, which in turn changes the mapping of the detector pixels onto reciprocal space by reorienting $\hat{\mathbf{x}}$ and $\hat{\mathbf{y}}$. For a given $k=|\mathbf{k}_i|=|\mathbf{k}_f|$ and $\alpha_i$, the value of the autocorrelation was evaluated for each point $(x,y)$ on the tangent plane of the Ewald sphere. This function $f(x,y,k,\alpha_f)$ describes the autocorrelation of the intensity distribution seen on the detector.

We computed images of this rod for a set of angles $\alpha_i$ using MATHEMATICA.[23] After some optimization with respect to the minor-axis dimension, the Gaussian ($\sigma$) width of the simulated rod was set to $\sigma_b=2.5\times10^{-5}$ Å$^{-1}$. Since this size is comparable with the spread of wave vectors present in the beam, we then further convolved each image $f$ with a distribution of $k$ to model the effects of the monochromator. The form of the $k$ distribution was also approximated by a Gaussian, with $\sigma_k/k=8.5\times10^{-5}$ chosen after some optimization of the comparison with data. This number corresponds also to the known $\Delta\lambda/\lambda$ of the beamline used.[18] The resulting series of model autocorrelation functions was then fitted to elliptical Gaussian functions in the same way as for the measured images.

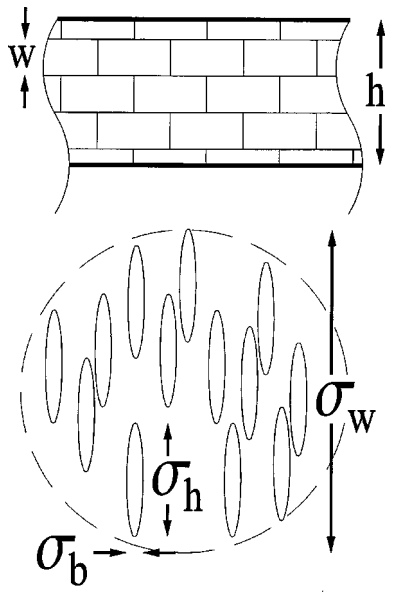


FIG. 5. Schematic description of the $Cu_3Au$ film in real space (top) and reciprocal space (bottom) based on our conclusions.

The orientation and elongation of the simulated images agree well with those observed in the experiment, as seen in Fig. 4. The elongation of the speckles as $\alpha_f$ approaches zero is clearly seen as the $\sigma$ width of the major axis of the elliptical Gaussians exceeds that of the minor axis by a factor of more than 10 when $\alpha_f=1°$. The fit to the observed orientation of the speckles becomes less reliable under conditions far from grazing exit because there is more experimental error when the speckles become round. Part of the systematic deviation of the orientation angles from the model may be due to the $k$ distribution differing from Gaussian. More significantly, the observed major-axis $\sigma$ lengths fall below those of the model (upper dashed curve) which diverge under the most grazing-exit conditions. This implies that, beyond the purely geometric considerations up to this point, there are contributions from the structure of the antiphase domains of the sample. The calculated distribution was therefore multiplied by yet another Gaussian to represent the distribution of scatterers in real space along the surface normal direction. By reciprocal-quadratic addition of the calculated $\sigma$ length with a constant value of $\sigma_h=(0.8\pm0.2)\times10^{-3}$ Å$^{-1}$ the lower dashed curve is obtained in Fig. 4, which coincides much better with the data. From this we conclude that the intensity autocorrelation function is finite rather than infinite in extent. In real space,[18] this corresponds to a length of $h=2900\pm700$ Å perpendicular to the surface, which is approximately equal to the known sample thickness. These details allow us to construct the sketch in Fig. 5, which shows the relevant length scales in both real and reciprocal spaces.

Our conclusion is therefore that the diffraction pattern of the antiphase domain structure consists of an assembly of long rods aligned along the surface normal, as supported by

the quantitative analysis given above. The fact that the model correctly reproduces the observed incidence-angle dependence of all aspects of the streaking allows us to identify the appropriate length scales labeled in Fig. 5. The typical size, $w = 400$ Å, of the antiphase domains, drawn schematically as blocks, determines the width of the envelope of the diffraction pattern, $\sigma_w = 5.9 \times 10^{-3}$ Å$^{-1}$.[18] The physical dimensions of the beam and the sample then determine the size of the speckles, as measured by their intensity autocorrelation function. These are $\sigma_h = 0.8 \times 10^{-3}$ Å$^{-1}$, as determined by the correction required to the major-axis length, and $\sigma_b = 2.5 \times 10^{-5}$ Å$^{-1}$ for the rod used in the simulation. The first number corresponds to a sample thickness of $h \simeq 2900$ Å while the second tells us that the effective beam size is 9.4 $\mu$m,[18] which is larger than the nominal 5-$\mu$m slit size used in the experiment because of the Fresnel diffraction by the blades.[24]

The dramatic streaking of the diffraction pattern is a characteristic of the grazing-*exit* geometry. Naively, this might have been expected under grazing-*incidence* conditions when the footprint of the small beam on the sample face would start to diverge; our calculation shows why just the opposite happens. We have demonstrated that varying the diffraction geometry allows us to measure systematically the three-dimensional extension of the 2D CXD pattern seen in the detector. A natural future extension of our method would be to sweep the energy, to allow the entire 3D diffraction pattern surrounding a superstructure reflection to be measured. It is hoped that, with the aid of iterative image-reconstruction techniques, the real-space structure of the entire illuminated region within the sample could be reconstructed, as our test calculations suggest.[25]

We are grateful for the assistance of P. Zschack at the UNICAT 33-ID beamline of the APS and would like to acknowledge R. Millane for valuable discussions. The UNICAT facility located at the APS is supported by the University of Illinois Materials Research Laboratory, Oak Ridge National Laboratory, the National Institute of Standards and Technologies, and UOP Research & Development. The APS is supported by the U.S. Department of Energy (D.O.E.) under contract No. W-31-109-ENG-38. The materials synthesis was funded by the D.O.E. under Contract No. DEFG02-96ER45439. J.A.P. wishes to acknowledge support from the U.S. National Science Foundation (NSF) under Grant No. DGE93-54978. The analytic part of this work was supported by the NSF under Project No. DMR98-76610.

[1] M. Sutton, S. G. J. Mochrie, T. Greytak, S. E. Nagler, L. E. Berman, G. A. Held, and G. B. Stephenson, Nature (London) **352**, 608 (1991).

[2] Z. H. Cai, B. Lai, W. B. Yun, I. McNulty, K. G. Huang, and T. P. Russel, Phys. Rev. Lett. **73**, 82 (1994).

[3] I. K. Robinson, R. Pindak, R. M. Fleming, S. B. Dierker, K. Ploog, G. Grübel, D. L. Abernathy, and J. Als-Nielsen, Phys. Rev. B **52**, 9917 (1995).

[4] J. L. Libbert, R. Pindak, S. B. Dierker, and I. K. Robinson, Phys. Rev. B **56**, 6454 (1997).

[5] O. K. C. Tsui, S. G. J. Mochrie, and L. E. Berman, J. Synchrotron Radiat. **5**, 30 (1998).

[6] S. Brauer, G. B. Stephenson, M. Sutton, R. Bruning, E. Dufresne, S. G. J. Mochrie, G. Grübel, J. Als-Nielsen, and D. L. Abernathy, Phys. Rev. Lett. **74**, 2010 (1995).

[7] S. B. Dierker, R. Pindak, R. M. Fleming, I. K. Robinson, and L. Berman, Phys. Rev. Lett. **75**, 449 (1995).

[8] T. Thurn-Albrecht, W. Steffen, A. Patkowski, G. Meier, E. W. Fischer, G. Grübel, and D. L. Abernathy, Phys. Rev. Lett. **77**, 5437 (1996).

[9] O. K. C. Tsui and S. G. J. Mochrie, Phys. Rev. E **57**, 2030 (1998).

[10] S. G. J. Mochrie, A. M. Mayes, A. R. Sandy, M. Sutton, S. Brauer, G. B. Stephenson, D. L. Abernathy, and G. Grübel, Phys. Rev. Lett. **78**, 1275 (1997).

[11] A. Malik, A. R. Sandy, L. B. Lurio, G. B. Stephenson, S. G. J. Mochrie, I. McNulty, and M. Sutton, Phys. Rev. Lett. **81**, 5832 (1998).

[12] D. Sayre, *Imaging Processes and Coherence in Physics* (Springer, Berlin, 1980).

[13] J. Miao, P. Charalambous, J. Kirz, and D. Sayre, Nature (London) **400**, 342 (1999).

[14] B. E. Warren, *X-ray Diffraction* (Addison-Wesley, Reading, Mass., 1969).

[15] P. Hirsch, A. Howie, R. B. Nicholson, D. W. Pashley, and M. J. Wheelan, *Electron Microscopy of Thin Crystals*, 2nd rev. ed. (Krieger, Malabar, FL, 1977).

[16] H. Reichert, P. J. Eng, H. Dosch, and I. K. Robinson, Phys. Rev. Lett. **78**, 3475 (1997).

[17] X.-M. Zhu, H. Zabel, I. K. Robinson, E. Vlieg, J. A. Dura, and C. P. Flynn, Phys. Rev. Lett. **65**, 2692 (1990).

[18] We have used the formula $\sigma = \sqrt{8 \ln 2}/L$ to relate the Gaussian width of a diffraction feature, $\sigma$, to the corresponding domain size, $L$, implying its full width at half maximum.

[19] S. W. Bonham and C. P. Flynn, Phys. Rev. B **58**, 10 875 (1998).

[20] Z. Cai, R. J. Dejus, P. D. Hartog, *et al.* Rev. Sci. Instrum. **67**, 3348 (1996).

[21] J. L. Libbert, J. A. Pitney, and I. K. Robinson, J. Synchrotron Radiat. **4**, 125 (1997).

[22] H. Dosch, B. W. Batterman, and D. C. Wack, Phys. Rev. Lett. **56**, 1144 (1986).

[23] S. Wolfram, *The Mathematica Book*, 3rd ed. (Cambridge University Press, Cambridge, 1996).

[24] I. A. Vartanyants, J. A. Pitney, J. L. Libbert, and I. K. Robinson, Phys. Rev. B **55**, 13 193 (1997).

[25] J. A. Pitney, I. A. Vartaniants, and I. K. Robinson, in *Proceedings of the SPIE Conference on Digital Image Recovery and Synthesis IV*, 1999, Vol. 3815, p. 199.